AGU PUBLICATIONS

Global Biogeochemical Cycles

RESEARCH ARTICLE
10.1002/2015GB005214

Key Points:
- The impact of ~1000 cyclones on marine production is explored in a global model and observations
- Chlorophyll responses to cyclones are mostly coastal in contrast with SST responses and only ~10% of induced blooms exceed 0.1 mg m-3
- The global impact of cyclones on primary production is ~1% of the annual production but shows regional contrasts

Correspondence to:
C. E. Menkes,
Christophe.menkes@ird.fr

Citation:
Menkes, C. E., M. Lengaigne, M. Lévy, C. Ethé, L. Bopp, O. Aumont, E. Vincent, J. Vialard, and S. Jullien (2016), Global impact of tropical cyclones on primary production, *Global Biogeochem. Cycles*, *30*, 767–786, doi:10.1002/2015GB005214.

Received 15 JUN 2015
Accepted 3 MAY 2016
Accepted article online 5 MAY 2016
Published online 27 MAY 2016

©2016. American Geophysical Union. All Rights Reserved.

Global impact of tropical cyclones on primary production

Christophe E. Menkes[1,2], Matthieu Lengaigne[2,3], Marina Lévy[2], Christian Ethé[2], Laurent Bopp[4], Olivier Aumont[2], Emmanuel Vincent[5], Jérôme Vialard[2], and Swen Jullien[6]

[1]Centre IRD, Nouméa, New Caledonia, [2]LOCEAN Laboratory, IPSL, Sorbonne Universités (UPMC, Univ Paris 06)-CNRS-IRD-MNHN, Paris, France, [3]Indo-French Cell for Water Sciences, IISc-NIO-IITM–IRD Joint International Laboratory, NIO, Goa, India, [4]LSCE-IPSL, CNRS/CEA/UVSQ, Gif-sur-Yvette, France, [5]Program in Atmosphere, Oceans and Climate, MIT, Cambridge, Massachusetts, USA, [6]Ifremer, Univ. Brest, CNRS, IRD, Laboratoire d'Océanographie Physique et Spatiale (LOPS), IUEM, Plouzané, France

Abstract In this paper, we explore the global responses of surface temperature, chlorophyll, and primary production to tropical cyclones (TCs). Those ocean responses are first characterized from the statistical analysis of satellite data under ~1000 TCs over the 1998–2007 period. Besides the cold wake, the vast majority of TCs induce a weak chlorophyll response, with only ~10% of induced blooms exceeding 0.1 mg m^{-3}. The largest chlorophyll responses mostly occur within coastal regions, in contrast to the strongest cold wakes that generally occur farther offshore. To understand this decoupling, we analyze a coupled dynamical-biogeochemical oceanic simulation forced by realistic wind vortices applied along observed TC tracks. The simulation displays a realistic spatial structure of TC-induced blooms and its observed decoupling with TC cold wakes. In regions of strong TC energy input, the strongest cold wakes occur in regions of shallow thermocline (<60 m) and the strongest blooms in regions of shallow nitracline and/or subsurface chlorophyll maximum (<60 m). Shallow thermoclines are found over many open ocean regions, while regions of shallow nitracline and/or subsurface chlorophyll maximum are most prominent in near-coastal areas, explaining the spatial decoupling between the cold and bloom wakes. The overall TC contribution to annual primary production is weak and amounts to ~1%, except in a few limited areas (east Eurasian coast, South tropical Indian Ocean, Northern Australian coast, and Eastern Pacific Ocean in the TC-prone region) where it can locally reach up to 20–30%. Nearly 80% of this TC-induced annual primary production is the result of the biogeochemical response to the 30% strongest TCs.

1. Introduction

In addition to their dramatic impacts on human societies, tropical cyclones (TCs) deeply affect the atmosphere and ocean structure. The physical response of the ocean to TCs has been well documented in recent decades. Intense TC winds cause vigorous upper ocean vertical mixing that cools the ocean upper layers while injecting warm surface waters downward [*Emanuel*, 2001; *Vincent et al.*, 2013] The efficiency of vertical mixing in cooling the ocean surface is enhanced by the vigorous upwelling occurring under the TC passage [*Jullien et al.*, 2012]. The amplitude of TC-induced cooling is obviously controlled by the amplitude of the TC energy input, which results from the combined effect of the TC intensity and translation speed [e.g., *Mei et al.*, 2012; *Vincent et al.*, 2012a]. However, the widely varying upper ocean precyclone stratification also modulates TC-induced cooling amplitude [*Lloyd and Vecchi*, 2010; *Neetu et al.*, 2012; *Vincent et al.*, 2012b; *Jullien et al.*, 2014], the TC-induced mixing being particularly efficient in cooling the ocean surface when the upper temperature profile is strongly stratified [e.g., *Vincent et al.*, 2013, and citations therein]. *Vincent et al.* [2013] further discussed the integrated impact of these TCs on the seasonal ocean thermal structure and heat transport: while they appear to have a marginal contribution to poleward heat transport, they contribute to a 10% reduction of the amplitude of the SST seasonal cycle within TCs basin. The TC-induced upwelling and vertical mixing are also likely to induce a chlorophyll increase by either providing nutrients to the surface layer and enhancing phytoplankton production or directly mixing an existing deep chlorophyll maximum upward. However, compared to the TC effects on temperature, much less is known about the TC effects on ocean biogeochemistry and biology. Due to limited observational means, the long-term biogeochemical response to TCs remains even more elusive than their local and individual impacts.

Remotely sensed surface chlorophyll observations nevertheless allowed several investigations of the regional surface chlorophyll responses to TCs. Very diverse responses, ranging from none to chlorophyll blooms, have

been reported under individual TCs but the relation between the amplitude of the response and the oceanic state under the TC remains unclear [*Shiah et al.*, 2000; *Lin et al.*, 2003; *Babin et al.*, 2004; *Lin*, 2012; *Zhang et al.*, 2014, to cite a few]. For instance, *Lin* [2012] observed 11 typhoons and their effects on ocean color during the 2003 summer in the western North Pacific and found that only two did induce a significant chlorophyll response (between 0.1 and 0.8 mg m^{-3}) while the others—among which some belonged to the strongest TC category (category 5)—did not. *Babin et al.* [2004] examined a series of TCs in a tropical region of the North Atlantic during 1998–2001 and also revealed a vast spread of responses, with chlorophyll increases ranging from 5 to 91%. These results suggest that the intensity of the observed surface chlorophyll response may result from a trade-off between the depth at which TCs mix the ocean and the depth of the nitracline and/or deep chlorophyll maximum.

Beyond the biogeochemical responses to individual TCs, another key question relates to the longer-term effect of these punctual, yet recurring phenomena. Extrapolating from one TC in the South China Sea, *Lin et al.* [2003] suggested that TCs could contribute to as much as 20 to 30% of the South China Sea climatological annual new production. The aforementioned diversity in the response to individual TC [*Babin et al.*, 2004; *Lin*, 2012] however illustrates the difficulty of extrapolating the long-term response from a single cyclone. Even if the local response to a TC may be large, TCs are rare and the potentially induced bloom only occupies a tiny fraction of the ocean surface [*Hanshaw et al.*, 2008]. One could nevertheless argue that strong TC activity areas are collocated with oligotrophic waters and could contribute to a relatively high portion of the annual production, as pointed out by *Babin et al.* [2004] for the North Atlantic. Yet *Lin* [2012] estimated that TCs did not contribute significantly to the annual primary production in the western North Pacific, one of the largest TC-prone region. Revisiting the North Atlantic in a region similar to that of *Babin et al.* [2004] but over a longer period (1997–2005), *Hanshaw et al.* [2008] concluded that TCs have a minimal effect ($<$1%) on the annual chlorophyll biomass because of their limited spatiotemporal influence. More recently, *Foltz et al.* [2015] suggested that the effect of TCs on interannual variations of the North Atlantic primary production was not negligible disagreeing with the results of *Hanshaw et al.* [2008] and pointing to potential biases in the data space-time resolution that they used. This lack of consensus hence raises the need to revisit the global long-term response of oceanic primary production to TCs and to mechanistically explain the diversity of chlorophyll responses under TCs.

So far, the vast majority of studies, if not all, have explored the ocean biogeochemical response to cyclones using observations. Exploring the responses to TCs in satellite observations is an obvious albeit difficult route, as these responses are often masked out/biased by clouds under TCs. On the other hand state-of-art ocean models are now helpful tools to explore both the local and long-term responses to TCs. Using a global ocean model, *Vincent et al,* [2012a, 2012b] developed an original numerical setting with which they could examine both the local and long-term global impacts of TCs on sea surface temperature (SST). Based on statistics built from the modeled response to ~3000 observed cyclones, they concluded that the amplitude of TCs cold wakes was essentially a function of two key parameters: an oceanic index representing the potential of the upper ocean to cool and a TC index representing the TC energy input into the ocean. This strategy also allowed [*Vincent et al.*, 2013] exploring the long-term contribution of cyclones to the global heat budget. *Lévy et al.* [2012] then used a setting similar to *Vincent et al,* [2012a, 2012b] but included a biogeochemical component to the ocean model. They could examine the effect of more than 1500 globally observed cyclones during 1993–2007 and assessed their long-term effect on air-sea CO_2 fluxes. They concluded that the overall effect of cyclones on regional climatological fluxes or their interannual variations was weak ($<$10%) due to several compensating effects.

In the present paper we aim at building on the aforementioned studies to explore the mechanisms underlying the individual and long-term surface chlorophyll/primary production responses to TCs regionally and globally over the 1997–2007 period. We will examine the SST and chlorophyll responses in parallel in this paper in both observations and a coupled global dynamical-biogeochemical model, in order to contrast mechanisms of the chlorophyll responses with those of the well-known SST response. After presenting the numerical setting, methodology, and comparing the model to observations (section 2), we will explore some individual cases (section 3) and show that the overall surface chlorophyll response can be linked to a number of key parameters (section 4). We will then assess the long-term effects of these powerful yet very episodic phenomena on the global primary production (section 5) and end by a summary and discussion of our results (section 6).

2. Methods

As mentioned in the introduction, previous studies examining the chlorophyll response to TCs relied almost exclusively on the analysis of remotely sensed chlorophyll data. We will also use ocean color data (section 2.1) and complement the data based analysis with that of an ocean simulation forced with realistic TC winds (presented in section 2.3). Our analyses cover a rather long time period (1997–2007), allowing to sample the ocean response to 1039 TCs globally and therefore to perform robust statistical analyses on the sensitivity of the amplitude to key TC characteristics and oceanic parameters (e.g., depth of the nitracline, section 2.2). We will also systematically compare the TC effects on SST and surface chlorophyll since they are likely to be affected by the same vertical processes.

We define the cyclonic seasons as April to December in the Northern Hemisphere and October to June in the Southern Hemisphere. This choice of such overlapping cyclonic seasons is based on the periods of maximum observed cyclone densities [*Menkes et al.*, 2012]. Changing the periods by 1–2 months does not change our results.

2.1. Observational Data Sets

Previous studies have used relatively high spatial resolution (4 km in *Lin* [2012] and *Foltz et al.* [2015] and 9 km in *Lin et al.* [2003], *Babin et al.* [2004], *Lin* [2012], and *Zhang et al.* [2014] for instance) with a diversity of time resolution such as daily in *Lin et al.*, [2003] and *Lin* [2012] who investigated individual responses to TCs in the North Pacific Ocean, 8 days in *Babin et al.* [2004], *Hanshaw et al.* [2008], and monthly in *Foltz et al.* [2015] who both aimed at assessing TC climatological impacts. We selected a daily resolution, which is the best possible resolution available for gridded ocean color data sets. In terms of spatial resolution, 4 km, 25 km, and 100 km resolutions are available from the GLOCOLOUR project (http://www.globcolour.info/products_description.html) or 9 km for SeaWiFs/MODIS ocean color databases (http://oceandata.sci.gsfc.nasa.gov/). Examination of chlorophyll blooms described in those studies shows that the TC-induced blooms exhibit horizontal spatial scales far larger than 9 km. Visual examinations of *Lin* [2012, Figure 3], *Lin et al.* [2003, Figure 1], and *Zhang et al.* [2014, Figure 11] reveal scales of order of ~100 km if not more. A composite analysis of the chlorophyll response under TCs (not shown) also reveals that the spatial scale of chlorophyll response under TCs is at least 250 km and similar to that of SST [see *Vincent et al.*, 2012b, Figure 7]. Hence, for our study assessing the impact of TCs worldwide, we chose to use the multisatellite merged global data product GLOBCOLOUR at daily and at 25 km resolutions (« CHL1 » GSM product, http://www.globcolour.info/products_description.html) rather than at higher spatial resolution. Such space/time resolution allows to resolve the main response scales and is in line with the ~50 km spatial resolution of our global model (see section 2.3). That aspect is discussed in section 6.

We use a blend of Tropical Rainfall Measuring Mission (TRMM) Microwave Imager (TMI) and Advanced Microwave Scanning Radiometer AMSR-E SST daily data set (http://www.ssmi.com/sst) at a ¼° horizontal resolution to characterize the observed SST responses under TCs as in *Jullien et al.* [2012] and *Vincent et al.* [2012b]. Despite their inability to retrieve SST data under heavy precipitation [*Wentz et al.*, 2000], TMI and AMSR-E offer the advantage of being insensitive to atmospheric water vapor and provide accurate observations of SST beneath clouds, a few days before and after the passage of a TC. The inner-core cooling (i.e., cooling under the eye) cannot be confidently assessed from TMI-AMSR because of the numerous missing data in a 400 km radius around the current TC position. This data set however provides a reliable estimate of the cooling in the TC wake, data being typically available 1 to 2 days after the TC passage. The world ocean database (http://www.nodc.noaa.gov/OC5/WOD05/pr_wod05.html) is finally used to estimate the background climatological hydrological and biogeochemical state under TCs. In particular, we use the 3-D chlorophyll data set, which is limited to a 100 m but allows retrieving the depth of the chlorophyll maximum above 100 m when it exists (see next section also).

We also used the cloud fraction (« CF » product, http://www.globcolour.info/products_description.html) to discuss some limitations of our results due to high cloud cover in the cyclone vicinities (see section 6) and it is useful to keep in mind that ocean color data are often missing under cyclones. Finally, we have punctually extracted Argo float hydrothermal profiles (http://www.argodatamgt.org/) to validate and discuss the model response in sections 3.1 and 4.

2.2. Useful Quantities Associated to TCs and Methodologies to Characterize Anomalies Under TCs

We employ a combination of two indices to understand the magnitude of the SST response under TCs. The first index is an atmospheric index related to the TC wind intensity. The second index is an oceanic one that

captures the upper thermocline depth. Two biogeochemical indices are extracted to constrain the chlorophyll response under TCs: the depth of the nitracline (DNO_3) and the depth of the deep chlorophyll maximum (DDCM). These indices are briefly described and discussed below.

2.2.1. Atmospheric Index: The Wind Power Index (WPi)

Vincent et al. [2012a] have developed the Wind Power index (WPi) using the definition of the power dissipation by friction associated with surface winds [*Emanuel*, 2005]. The WPi is a proxy for the amount of kinetic energy transferred to the ocean by the cyclone, i.e., the amount of energy available for mixing under the storm. For our specific purposes, we have arbitrarily classified WPi into five categories ranging from Cat 1 ($0 < \mathrm{WPi} < 1$: weakest storms) to Cat 5 WPi ($\mathrm{WPi} > 5$, strongest storms). A detailed description of the WPi index computation and of its physical meaning is found in *Vincent et al.* [2012a]. They have shown that this quantity allows better discrimination the oceanic response under TCs than the classical Saffir-Simpson scale (see their Figure 6). The same conclusion holds for the chlorophyll response (not shown). This can easily be explained by the fact that WPi accounts for both the maximum winds and translation speed of the storms, which are both important for the oceanic response: slowly moving and intense storms transfer the largest amount of energy to the ocean and result in higher SST and chlorophyll responses than for instance fast moving and intense storms.

2.2.2. Oceanic Index: The Upper Thermocline Depth (H2)

Lloyd and Vecchi [2010] have shown that the depth of the SST minus 2°C isotherm (hereafter H2) is a good parameter for estimating the amplitude of the SST response to TCs. This parameter accounts for the ocean efficiency to respond to vertical mixing, deeper H2 being associated with weaker cooling for a given TC. *Vincent et al.* [2012a] further showed that H2 and WPi rank among the best combination to predict the TC cooling amplitude from the TC and ocean background state characteristics.

2.2.3. Nitracline and Deep Chlorophyll Maximum Depths

The main mechanisms responsible for the occurrence of chlorophyll blooms under TCs are either new nitrate injection from the nitracline and/or chlorophyll injection from a deep chlorophyll maximum by mixing/upwelling [*Babin et al.*, 2004; *Hanshaw et al.*, 2008; *Lin,* 2012]. We estimate the depth of the nitracline (DNO_3) as the depth where NO_3 increases above 1 μm. If surface NO_3 exceeds this threshold, DNO_3 is set to zero. The nitracline depth is a natural index to consider since most regions under the influence of TCs are nitrogen limited [*Moore et al.*, 2013]. It is the equivalent of the thermocline depth when looking at SST responses under TCs. We also calculate the depth of the deep chlorophyll maximum (DDCM), which can be mixed up/upwelled in the upper ocean under TCs and could participate to observed blooms [*Babin et al.*, 2004]. Note that the depth of DCM deeper than 100 m cannot be derived from observations, as the World Ocean Atlas Database does not provide chlorophyll values below this depth.

2.3. Coupled Dynamical (NEMO)-Primary Production (PISCES) Model

2.3.1. Model Description

We use the same dynamical-biogeochemical configuration as that in *Lévy et al.* [2012], with an identical forcing strategy. Briefly, the ocean model is built from the "Nucleus for European Modeling of the Ocean" (NEMO v3.2) ocean/sea-ice numerical framework [*Madec*, 2008]. The model configuration (known as ORCA05) uses a tripolar, quasi-isotropic grid with a nominal resolution of 1/2°. It has 46 vertical levels, with 10 levels in the upper 100 m and 250 m resolution at depth. It is coupled online to the Pelagic Interaction Scheme for Carbon and Ecosystem Studies (PISCES) [see *Aumont and Bopp*, 2006] that includes a simple representation of the marine ecosystem and describes the cycles of carbon and of the main marine nutrients (N, P, Fe, and Si). The model has 24 compartments. Four living pools are represented: two phytoplankton size classes/groups (nanophytoplankton and diatoms) and two zooplankton size classes (microzooplankton and mesozooplankton). Fixed Redfield ratios are employed for N and P, while the ratios of both Si, and Fe, to C vary dynamically as a function of the phytoplankton functional group and environmental variables.

2.3.2. Model Setup and Experimental Design

The surface boundary conditions are based on the second version of the atmospheric data sets and formulations developed by *Large and Yeager* [2009] for global ocean-ice models and are referred to as CORE V2 from the Coordinated Ocean-ice Reference Experiments (CORE) forcing [*Griffies et al.*, 2009]. The forcing data sets are based on a combination of NCEP/NCAR reanalysis products with various satellite data sets and involve adjustments that correct global imbalances (e.g., produce near-zero global mean heat and freshwater fluxes when used in combination with observed SSTs). Turbulent fluxes are computed from the CORE bulk formulae

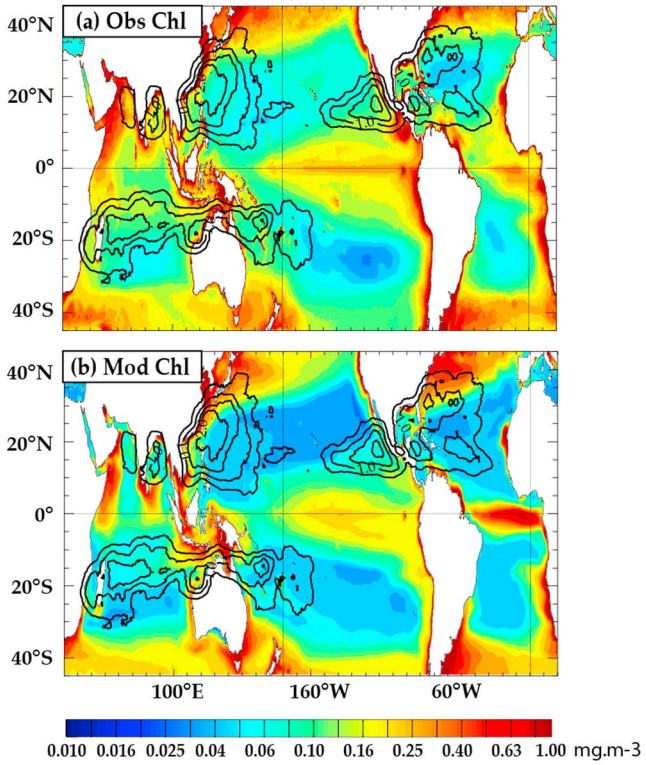

Figure 1. Climatological surface chlorophyll (color; in mg m^{-3}) and WPi (contour, every 0.5) from (a) observations and (b) model over the cyclonic seasons (defined as April to December in the Northern Hemisphere and October to June in the Southern Hemisphere). Note the log scale on the color bar.

as a function of the prescribed atmospheric state and the simulated ocean surface state (SST and surface currents). Following *Donelan et al.* [2004], we introduced a saturation of the CORE dimensionless surface drag coefficient (C_D) for winds in excess of 33 m s^{-1}, to account for its observed behavior at strong winds. Data are prescribed at 6-hourly (wind speed, humidity, and atmospheric temperature), daily (short- and long-wave radiation), and monthly (rain and snow) resolutions, with interannual variability for all input variables except runoff, which is climatological. To avoid an artificial model drift due to a freshwater imbalance, sea surface salinity is restored toward monthly mean climatological values with a piston velocity of 50 m/300 days. Boundary conditions for the biogeochemical model include atmospheric dust (Fe) deposition, rivers (Fe, N, P, Si, and C) and a crude parameterization of sediment (Fe) mobilization at the coasts. These sources, described in more details in *Aumont and Bopp* [2006], are kept constant during the simulation.

We use the last timestep of a 60-year ORCA05-PISCES global simulation as initial conditions and start our simulation in 1995. The CORE forcing strongly underestimates the wind signals under TCs. The 10-m wind forcing of the present simulation is modified to include TC forcing following *Vincent et al.* [2012b] as follows. The CORE wind forcing is first filtered in the vicinity of observed TCs tracks in the IBTrACs database (http://www.ncdc.noaa.gov/oa/ibtracs), in order to suppress the weak cyclone signal there. The TC wind signal is then added, based on the *Willoughby et al.* [2006] idealized vortex spatial structure, which is based on a statistical fit to observed TC winds [*Willoughby and Rahn*, 2004]. This analytic wind forcing is applied at every time step, by temporally interpolating the 6-hourly positions of the cyclones in IBTrACs. This approach corrects for the underestimation of TC winds in CORE. An illustration of the procedure is provided in *Vincent et al.* [2012b, Figure 1]. We discard the first 3 years of the simulation when the upper ocean is still adjusting to the forcing and examine the 1998–2007 10 year outputs. The 1039 cyclones are sampled over that period. Daily outputs are used for the analyses of surface parameters. In the paper, depth-integrated primary production (also a daily output) is simply referred to as primary production. Monthly outputs are used for subsurface ocean analyses.

The average WPi pattern (contours in Figure 1) highlights regions where most TCs occur. In these regions, waters are mostly oligotrophic (Figure 1a) and the model compares favorably with observations (Figure 1 b). The model underestimates chlorophyll along the coast of Peru and Chile and overestimates chlorophyll in the Atlantic equatorial upwelling, but these biases are not located in TC-prone areas and therefore unlikely to affect the conclusions drawn from our model results.

3. Local Response Under TCs

3.1. Case Studies of TCs Ketsana and Parma

In this section, we qualitatively examine the observed and modeled cold wake and bloom response to the Ketsana and Parma TCs (Figure 2). Both TCs occurred during the 2003 cyclonic season in the Northwest

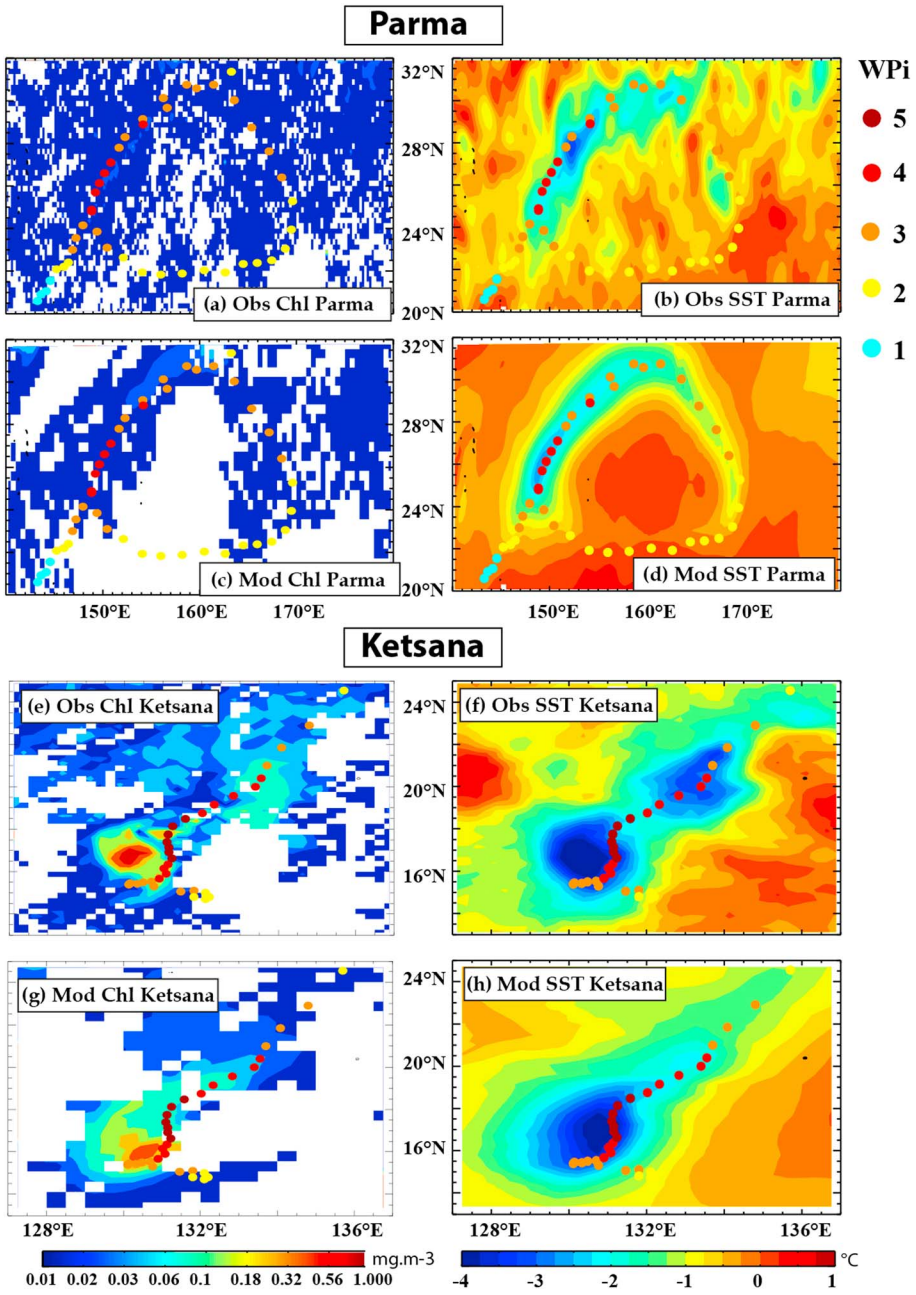

Figure 2. (a–d) The 7 day mean seasonal anomaly of ocean response under the category 4 typhoon Parma between in the Western Pacific between 27 October 2003 and 2 November 2003. (e–h) Same as above but for the Typhoon category 5 Ketsana in the Western Pacific, using the 7 day mean from 22 October to 29 October 2003. In each panel, the mean over −10 to −3 days before cyclone passages is removed consistently with the other analyses (see methods). Also, the model has been masked in grid points where observations were not available. (Figures 2a–2d) Observations of (Figures 2a and 2c) chlorophyll (mg m^{-3}) and (Figures 2b and 2d) SST (°C). (Figures 2e–2h) Same but for the modeled response. The dots represent the cyclone track, with colors indicating the WPi value as indicated by the color code on the right-hand side of the figure. Note the log scale for the chlorophyll.

Pacific and have been analyzed by *Lin* [2012]. These two TCs are interesting to compare because of their contrasted chlorophyll responses.

Parma exhibits a very peculiar anticyclonically rotating track. It became a storm near 20°N on 20 October 2003 and reached its maximum WPi amplitude (Cat 5, note that we use the WPi categories as detailed in section 2.2) on 29 October, when passing near its initial position again. It then weakened to Cat 2 as it

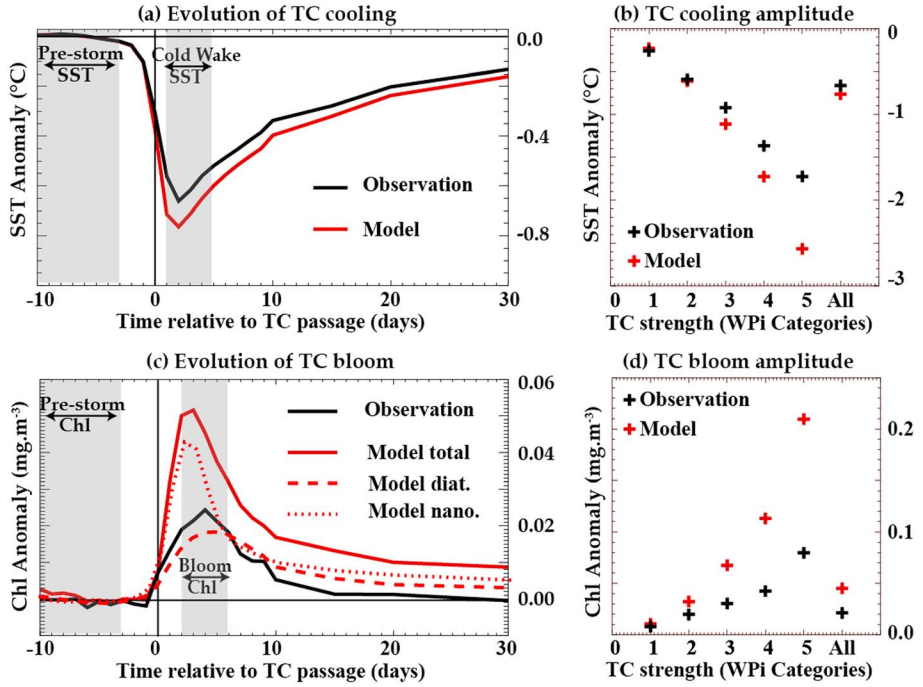

Figure 3. (a, c) Composite evolution of TC-induced (a) cooling and (c) chlorophyll responses along TC tracks from 10 days before to 30 days after the TC passage. Anomalies are calculated with respect to average prestorm values (days −10 to −3) over a 200 km radius from the TC's position. Day 0 refers to the time of the TC passage. This composite is built from 1039 storms over the 1998–2007 period. For the model chlorophyll, the different curves in red represent the two phytoplankton species as well as the total chlorophyll as labeled in the panel. (b, d) Amplitude of TC-induced (b) cooling and (d) chlorophyll response as a function of WPi categories as well as the mean response over all categories. The amplitude of the response is taken as the averaged anomalies from days +1 to +5 for SST and +2 to +6 for chlorophyll (see grey shadings in Figures 3a and 3c). Units are in °C for SST and in mg m^{-3} for chlorophyll. Model curves in Figures 3a and 3c are in red.

moved near 32°N on 31 October. Ocean color observations show no noticeable chlorophyll response during Parma (Figure 2a) despite clear cooling signals along its track: the maximum cooling (~2°C at its maximum) is observed during the last days of October when it reached Cat 5 WPi (Figure 2b). The model provides a consistent picture with satellite observations, i.e., the absence of a chlorophyll response (Figure 2c) and a cooling of similar amplitude albeit with a clearer signal along the entire TC track (Figure 2d).

Ketsana moved northeastward. It became a storm on 19 October and quickly intensified into a typhoon on 20 October to reach its maximum Cat 5 WPi on 22 October. In contrast with Parma, Ketsana induced a chlorophyll bloom between 21 October and 22 October [see also *Lin*, 2012], with observed values reaching more than 0.8 mg m^{-3} to the left of the track where the storm entered Cat 5 WPi (Figure 2e). It also induced an intense cooling, reaching ~ −5°C (Figure 2f), to the left of the storm. While the largest cooling near 16°N–130°E is well captured by the model, the modeled cold wake does not exhibit a secondary cooling near 20°N–134°E as in the observations. This discrepancy can be tracked back to differences between model and observed upper ocean stratification depth (derived from H2 parameter introduced in section 2.2): the available Argo floats within 20 days before the cyclone passage near that location indeed indicate that modeled H2 in the region is approximately 30 m deeper than in the observations (not shown). Such a model bias potentially due to a mesoscale structure in observations that cannot be reproduced at the same location in the model largely explains the underestimated TC-induced cooling amplitude [*Vincent et al.*, 2012b]. In section 4, we will discuss more precisely that bias by illustrating how the response amplitude varies with H2 and other parameters. The modeled chlorophyll wake has similar spatial structure than the modeled SST, being slightly closer to the TC track than in observations (Figures 2g and 2h). Interestingly, model and data chlorophyll responses do not show a secondary bloom, in the region where the secondary cooling is evident in observations (Figure 2f). This point will also be further discussed in section 4.

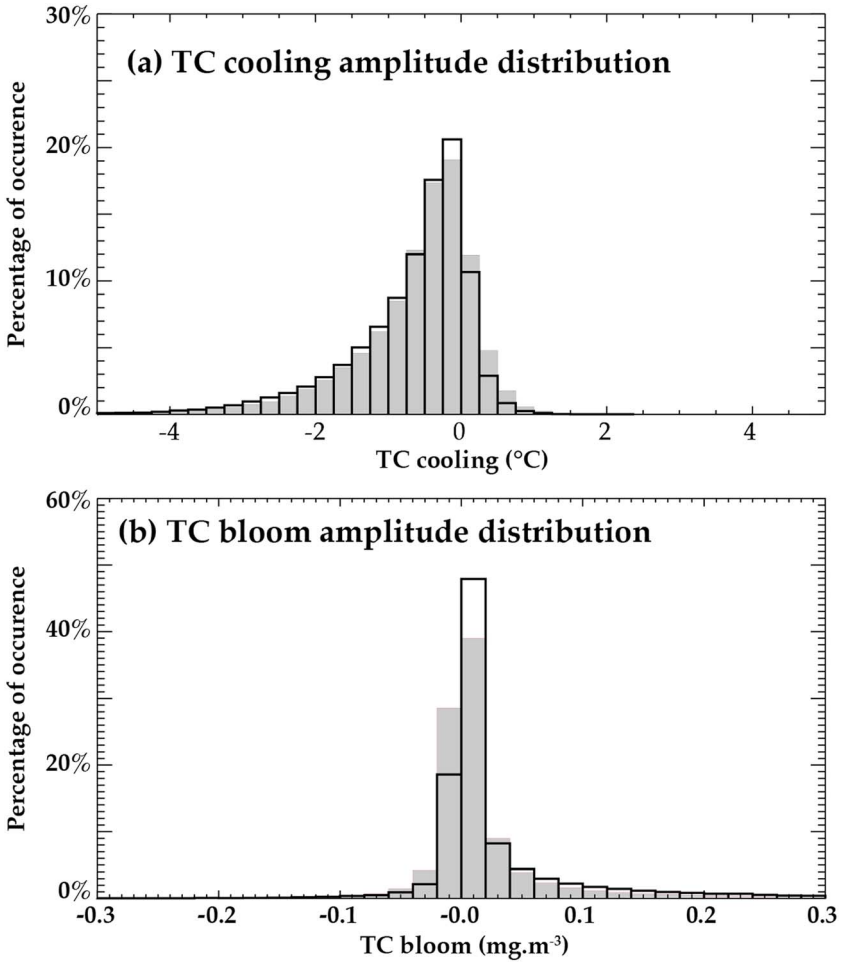

Figure 4. Normalized distributions of (a) SST and (b) chlorophyll responses under TCs (in 200 km radius, see text) in observations (shaded grey) and in the model (black). The *x* axis has been purposely limited to the main responses but outliers also exist in the distributions. The amplitude of the response refers to the signal averaged between days +2 to +5 from the cyclone passage for chlorophyll and from day +1 to +4 for the SST, relative to the average situation between 10 and 3 days before the TC passage (see Figure 3 and legend).

3.2. Responses Under TCs at Global Scale

The two examples above illustrate the diversity of the ocean response to TCs. To assess the SST and chlorophyll responses under TCs, we further analyze the time evolution and amplitude distribution of the composite response of TC-induced SST and chlorophyll signals (Figures 3 and 4).

The model and observations provide very similar estimates of the timing and amplitude of the mean SST response to TCs (Figure 3a). This SST response has been extensively discussed in *Jullien et al.* [2012], *Lévy et al.* [2012], and *Vincent et al.* [2012b]. In line with their results, we find that SST starts cooling 3 days before the TC passage (day −3), with a maximum cooling occurring 2 days after its passage (day +2). The cooling starts decreasing from day + 2 onward but persists for at least 30 days after the cyclone passage. Hereafter, the cold wake amplitude is defined as the difference between the cold wake (day +1 to day +4) and the prestorm (day −10 to day −3) SST average values (see grey shadings in Figure 3a). Figure 3b reveals that while the amplitude of the modeled cooling is in good agreement with observations for weakest TCs (WPi weaker than 3), the model overestimates the cooling amplitude for the strongest TCs (WPi equal or larger than 3). The amplitude of the signal averaged over all categories is however found to be similar between model and observations (Figure 3b), which can be explained by the fact that 85% of the cyclone days are due to WPi category 1–3 (see Figure 11c and section 5). Figure 4a also illustrates that in addition to a realistic mean SST response, the modeled distribution of the individual responses also compares very well with observations. In both the model

and the observations, most of the cold wakes indeed exhibit a rather weak amplitude (~75% of the coolings are weaker than −1°C) while intense cold wakes are less frequent (~7% of the coolings exceed −2°C).

Figure 3c shows that an increase in chlorophyll also occurs on average under TCs for both model and observations. This bloom starts at the time of the TC passage and peaks 3 to 4 days later. The bloom lasts about 2–3 weeks in the data, a time scale consistent with previous studies using 8 day data [*Babin et al.*, 2004; *Hanshaw et al.*, 2008]. In the model the early bloom period is dominated by small (pico-nano) plankton (Figure 3c). Larger plankton (diatoms) can contribute up to 50% of the total model bloom a week after the TC passage. While the small plankton peaks at day 2, the diatom response peaks between days 4 and 6. The maximum chlorophyll response lags that of SST by 1 day in the model (Figure 3a) and 2 days in the observations. There is however a clear difference between modeled and observed blooms, with twice as large a bloom in the model than in observations (~0.05 mg m^{-3} against ~0.025 mg m^{-3}). We define the bloom amplitude as the difference between the average chlorophyll during the maximum of the bloom (day +2 to day +5) and during the prestorm (day −10 to day −3; see grey shadings in Figure 3c). Choosing other reasonable averaging time periods slightly changes the amplitude of the responses discussed farther in the paper, but not our overall conclusions. When stratifying the amplitude of the bloom as a function of WPi categories (Figure 3d), model and observations exhibit a similar tendency of larger blooms with increasing TC intensity. The model however overestimates the amplitude of the bloom for WPi larger than 1.

The distribution of individual TC bloom amplitudes is shown in Figure 4b. The modeled and observed bloom distributions are qualitatively similar with a large proportion of weak TCs chlorophyll responses (60% of the responses range between −0.02 and 0.02 mg m^{-3}). The larger bloom amplitude in the model seen in Figure 3 b largely arises from two factors. First, negative chlorophyll responses occur more frequently in the observations (37% of the responses) than in the model (20% of the responses). Possible reasons for these negative values are discussed in section 6. Second, intense blooms occur more frequently in the model than in observations (16% of the blooms exceed 0.1 mg m^{-3} in the model against 8% in the observations). In an attempt to understand that discrepancy, we resampled the model as the observations by discarding model values when corresponding observational data were missing, but this did not significantly change the amplitude between the two data sets, suggesting that the amplitude mismatch between the model and observations is real and not an artifact due to spatiotemporal sampling.

Figure 5 displays the spatial distribution of the TC cold wakes and blooms amplitude for the model and observations. These maps are produced by averaging the maximum cooling and bloom amplitude during a TC passage for all points within 200 km of each TC position and during each TC season and then averaging those seasonal maps over the 1998–2007 period. The model average TC-induced cooling pattern (Figure 5b) agrees generally well with the observed one (Figure 5a). There is also a good coherence between the modeled and observed chlorophyll response patterns, as well as a reasonable amplitude agreement at the global scale (Figures 5c and 5d). The model however generally overestimates the amplitude of the chlorophyll response to TCs, especially in the South China Sea and Northeast Pacific. Interestingly, the spatial pattern of the chlorophyll response is very different from that of the SST response, with maximum chlorophyll responses being strikingly more confined closer to the coasts than the cold wakes in both the model (Figures 5b and 5d) and the observations (Figures 5a and 5c). For instance, the North Pacific north of 20°N is a region of strong cold wakes off the coasts, while the maximum chlorophyll blooms are mostly confined within ~1000 km of the coast. This suggests that different factors control the amplitude of the cooling and bloom under a given TC.

4. Factors Controlling the TC Wake Amplitudes and Spatial Patterns

In this section, we will first qualitatively show that intense TC coolings occur in regions with both a high WPi and a shallow thermocline (measured from H2). Similarly, we will show that blooms occur in regions with both a high WPi and a shallow nitracline (DNO_3)/deep chlorophyll maximum (DDCM). This qualitative explanation of the cooling/chlorophyll response spatial patterns will be followed by a more quantitative estimate of their relations with WPi, H2, DNO_3, and DDCM.

The WPi introduced by *Vincent et al.* [2012a] is a measure of the energy transferred by the cyclone to the upper ocean and available for vertical mixing. *Vincent et al.* [2012a] have shown that the WPi is an important factor for determining the ocean thermal response to the TC. The maximum cold wake amplitudes are mostly

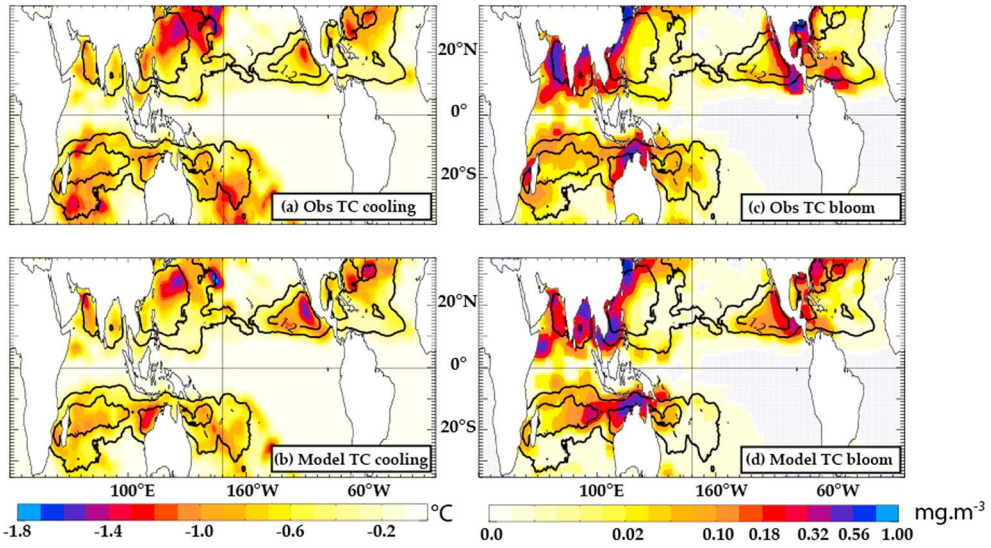

Figure 5. Observed (a) averaged TC-induced cooling (in °C) and (b) averaged chlorophyll response (in mg m^{-3}). (c, d) Same for the model. The SST map is constructed by taking the maximum SST response under TCs over a radius of 200 km and during days +1 to +4 after the TC passage minus the same mean but during days −10 to −3. The chlorophyll map is constructed by taking the maximum chlorophyll response under TCs over a radius of 200 km and during days +2 to +5 after the TC passage minus the same mean but during days −10 to −3. Those maps are constructed over each cyclonic season (defined as April to September in the Northern Hemisphere and October to March in the Southern Hemisphere) over the 1998–2007 period. Note that the color scale for the chlorophyll response is logarithmic. The WPi 0.4 and 1.2 contours are shown on all panels, to highlight TC-prone regions.

located in the main WPi areas (Figures 5a and 5b), highlighting the crucial role of wind energy input to the ocean in setting the amplitude of the cooling. A closer look however reveals that maximum TC-induced coolings are not systematically collocated with maximum WPi. The maximum cooling, for instance, occurs poleward of the maximum energy input in the Northwestern and Southwestern Pacific. This suggests that other factors than the TC strength control the amplitude of the TC-induced cooling. *Vincent et al.* [2012a] showed that the TC cooling is the result of the combination of two factors: the energy transferred to the ocean by the cyclone (WPi) and the oceanic stratification, as depicted by the H2 oceanic parameter described in section 2. Low values of H2 indicate regions where cool waters are close to the surface and where the ocean is prone to surface cooling by oceanic vertical mixing. The spatial distribution of the average TC cooling can thus be explained by the combined spatial distribution of WPi and H2 at first order.

Figures 6a and 6b show that the climatological H2 patterns are very consistent between the model and observations. The highest values of H2 are found in the Western Pacific warm pool where the thermocline is deep, while upwelling regions such as the Eastern equatorial Pacific or a northeasterly orientated band between 20°N and 30°N in the Northwest Pacific and Atlantic are characterized by low H2. This spatial structure of H2 imposes an additional constraint to that of the WPi on the spatial structure of the cooling pattern: within high WPi regions, strongest cold wakes indeed occur where H2 is weakest (<~60 m), i.e., north of 20°N in the Northwestern Pacific and Atlantic and offshore of the western coast of Central America.

The WPi also exerts a strong control on the chlorophyll response to TCs: responses indeed only occur within the 0.4 WPi contour (Figures 5c and 5d). But while WPi values above 0.4 extend far into the open ocean, the major areas of strongest TC-induced blooms are confined near the coasts. For instance, the Northwest Pacific east of 140°E or the Northwest Atlantic are associated with large TC energy input but include large regions of weak chlorophyll responses. This results in a weaker correlation pattern between WPi and TC blooms (~0.5, $p < 0.01$) than that between WPi and TC cooling (~−0.7, $p < 0.01$). This suggests that the TC wind energy input to the ocean cannot explain the amplitude of the bloom alone. In line with previous studies, we consider two oceanic parameters to explain the chlorophyll blooms in combination with WPi. The depth of the nitracline (DNO_3) is important, as it will determine whether the cyclone can easily bring up nitrate into the euphotic layer for chlorophyll production. Mixing/upwelling associated with a given cyclone will indeed more easily enrich the mixed layer with nutrients if the nitracline is relatively shallow. But the cyclone can also

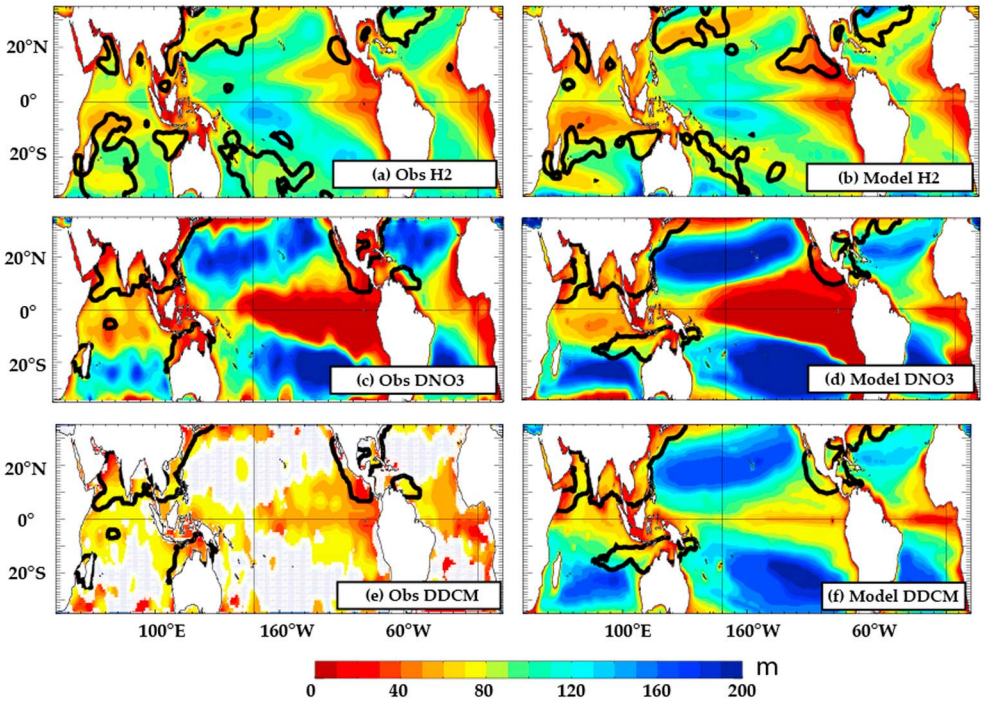

Figure 6. Climatological depth (in meters) of (a) upper thermocline (H2) and (c) nitracline (defined as the 1 μm; DNO_3) for the TC-prone seasons. (e) Mean depth of the DDCM. (b, d, and f) Idem but for the model. Note that in Figure 6e, regions where the DDCM is lower than 100 m cannot be calculated in the data and are left blank (see also data section). The −0.8°C TC cooling contour, estimated as in Figure 5, is shown in Figure 6a for observations and Figure6 b for the model. The 0.05 mg m^{-3} TC chlorophyll response contour (estimated from Figure 5) is shown in Figures 6c and 6e for observations and Figures 6d and 6f for the model.

enrich surface chlorophyll by mixing upward an existing subsurface chlorophyll maximum [*Babin et al.*, 2004; *Hanshaw et al.*, 2008; *Lin*, 2012; *Foltz et al.*, 2015]. We will hence also consider the depth of the deep chlorophyll maximum (DDCM). These two oceanic variables can be considered as the chlorophyll counterparts of H2 for the cold wake amplitude.

Similarly to Figures 6a and 6b, Figures 6c and 6d present the modeled and observed DNO_3 and Figures 6e and 6f the DDCM. A deep nitracline is found in the tropical gyre centers and a shallower nitracline in the equatorial regions and near the coasts in both the model and the observations (Figures 6c and 6d). The modeled and observed nitraclines match very well, with a pattern correlation equal to 0.84 ($p < 0.01$). The model however exhibits a slightly deeper nitracline in the North Pacific and South Indian Ocean tropical gyre centers. Both modeled and observed DDCM data also show agreeing patterns with values in the TC response areas that are similar. Note that the DDCM and DNO_3 also have similar spatial patterns (0.85 correlation, $p < 0.01$). Similarly to DNO_3, the DCM is shallower in coastal and in all the main upwelling regions and deeper in the center of the tropical gyres (Figure 6f). At first order, deep chlorophyll maxima occur at depths where both light and nutrients are available, i.e., at the intersection between the euphotic layer and top of the nitracline. The DDCM is hence generally located at the top of the nitracline, which is shallower than DNO_3 with our choice of the isopleth criterion for that quantity (Figures 6e and 6f).

Interestingly, Figure 6 shows that an additional necessary condition to WPi > 0.4 for TC-induced blooms is DNO_3 and DDCM shallower than approximately 80 m (which essentially occurs near the coasts within regions where WPi > 0.4). For instance, the average TC-induced bloom never reaches more than 0.05 mg m^{-3} in regions with a large WPi and a nitracline deeper than 150 m, as this the case for the central North Pacific for example.

The comparison between the panels of Figure 6 shows that there is a qualitative agreement between H2 and DNO_3/DDCM near the coasts where all fields exhibit low values, but this relation is far less evident in the center of the gyres. In these regions, DNO_3/DDCM is considerably deeper than the corresponding H2 values.

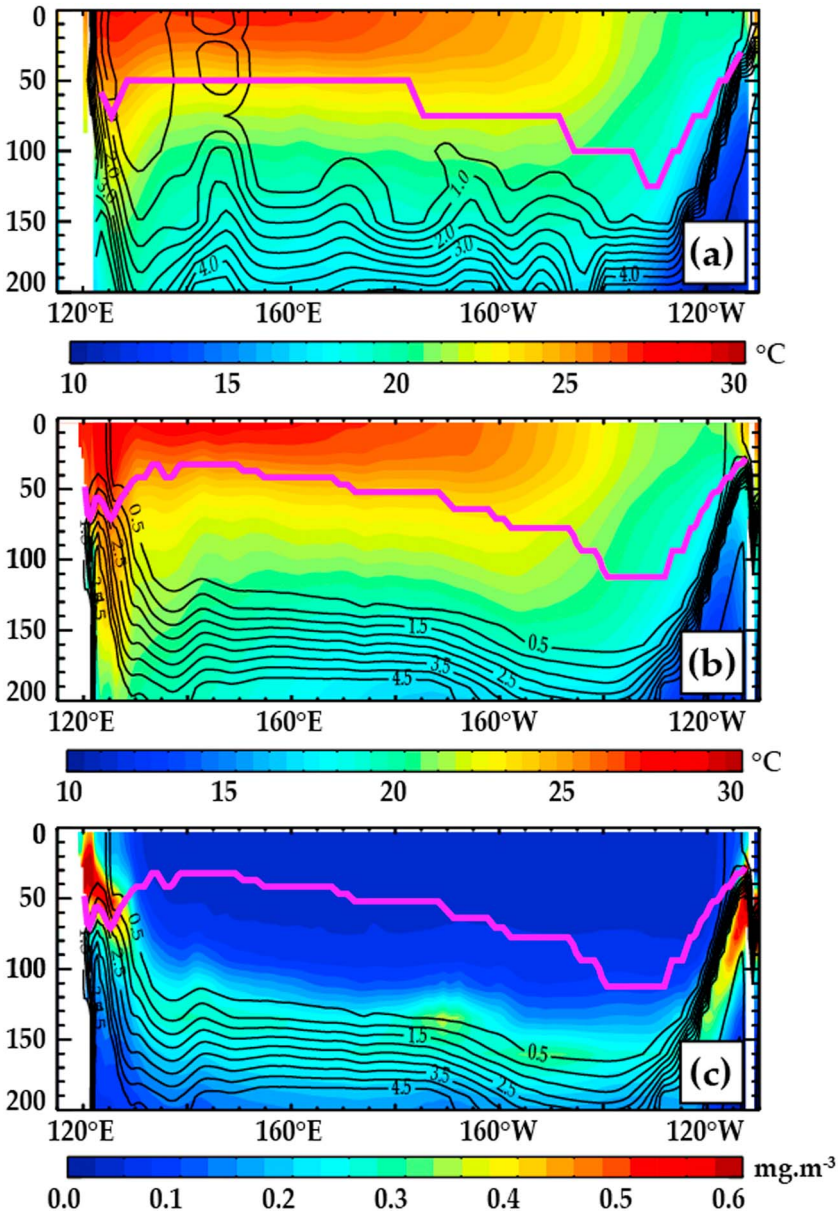

Figure 7. Vertical zonal section along 25°N in the Pacific of (a) observed and (b) modeled temperature (color, in °C) and nitrate (contour, in μm) and (c) of chlorophyll (color; in mg m^{-3}) and nitrate (contour; in μm) for the model. In all panels, the pink curve indicates H2 (observed for a and modeled in Figures 7b and 7c).

TC-induced cooling can hence be large in these regions because the upper thermocline (H2) is shallow enough (<80 m) to allow mixing/upwelling induced by TC winds to cool the ocean surface. On the other hand, DNO_3 and DDCM are too deep in the gyre centers (>160 m) to allow either nitrate or chlorophyll injection into the surface layer by TC-induced mixing/upwelling. That is illustrated in Figure 7 where differences in the vertical structure of temperature, nitrate, and DCM for the Northern Pacific along 25°N are presented. At that location, the model and observations both display a temperature decrease from the surface, with a sharper stratification (H2) between 30 and 70 m depth, resulting in a H2 located around 50 m depth between 120°E and the dateline (Figures 7a and 7b), i.e., in the TC-prone region. This allows TC wind forcing to efficiently cool the ocean surface there. In contrast, the upper ocean is completely nitrate depleted down to 100 m east of 130°E, resulting in a nitracline located around 150 m. There is an upward tilt of the nitracline near the coast between 120°E and 130°E, with large nitrate concentrations near the surface which favors large blooms when TCs pass there. Similarly, the DCM is deep between the dateline and 130°E, while it shoals

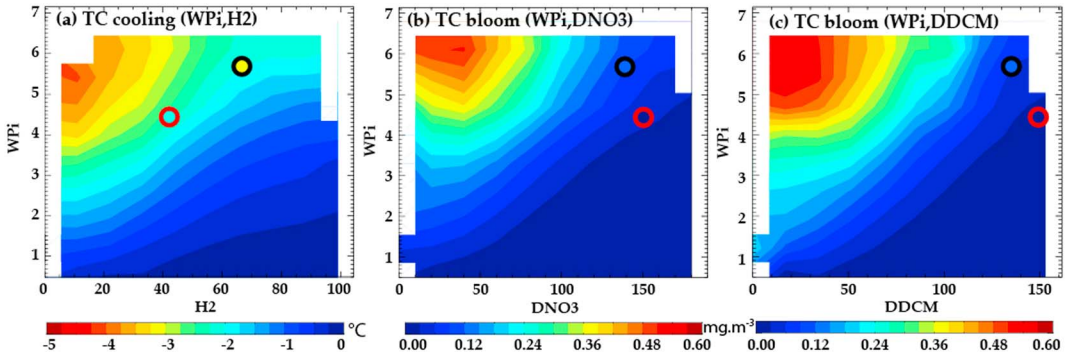

Figure 8. Amplitude of modeled TC-induced (a) cooling as a function of WPi and H2, (b) chlorophyll response as a function of WPi and DNO_3, and (c) chlorophyll response as a function of WPi and DDCM. The responses are binned in 10 equal segments for each variable. Results are not sensitive to the bin size. Bins are only considered when 10 samples or more are available. The color dots represent Ketsana (black contour) and Parma (red contour) at the time of their maximum cooling (21 October 2003 for Ketsana and 29 October 2003 for Parma) in the parameter space: the color within each circle denotes the actual response amplitude.

rapidly when reaching the east coast of the Eurasian continent (Figure 7c). These differences in temperature and nitrate vertical structure largely explain the differences in the TC-induced cooling and bloom patterns (Figure 5).

We will now explore the relationships between the TC-induced bloom/cooling and WPi/oceanic parameters more quantitatively. The following analyses are only performed from the model outputs, as we do not have access to observed H2, DNO_3, and DDCM under TCs. To better quantify the respective roles of the TC characteristics and ocean background state in setting the amplitude of the ocean response we first tried to fit the modeled responses as a function of two key parameters: TC strength (i.e., the WPi) and ocean parameters (H2 for TC-induced cooling and DNO_3 and DDCM for TC-induced blooms). It is not possible to obtain any significant fit, as the response dispersion is too large. To reduce the dispersion, we thus proceeded as in [*Vincent et al.*, 2012a] as follows: we binned the amplitude of the TC cold wakes and blooms as a function of the two parameters. First the parameter ranges are divided into 10 equal segments. For instance, H2 varies down to 100 m and is thus divided into 10 m segments (see Figure 8 axes for the parameter ranges). Within each bin in the two-parameter space, modeled responses are averaged and shown in Figure 8 (we also keep track of the response variability within each bin as explained in the following). The responses in a given bin are discarded when they contain less than 10 TC observations.

Figure 8a illustrates the cold wake amplitudes binned as a function of WPi and H2. As previously mentioned, the average cooling increases as a function of WPi and decreases as a function of H2. Large cooling (>2°C) only occurs when powerful TCs (WPi > 2.5) travel over a very stratified upper ocean (H2 < 60 m). A similar analysis is then performed for the TC-induced blooms binned as a function of WPi and DNO_3 (Figure 8b) and of WPi and DDCM (Figure 8c). This analysis shows an overall increase of the bloom amplitude in the TC wake with increasing WPi and decreasing DNO_3/DDCM. It is also worth pointing out that strongest blooms (>0.2 mg m^{-3}) are confined to regions where $DDNO_3$/DDCM is lower then ~100 m.

The difference in behavior of TC cooling and blooms under Ketsana and Parma, the two examples of Figure 2, can now be understood with the help of Figure 8. First, as reported in section 3.1 and Figure 2, the model SST response to Ketsana does not exhibit a secondary cooling near 134°E–20°N as in observations. The Argo data clearly show that the ocean observed preconditioning H2 was at ~50 m in the data and ~80 m in the model (not shown), more than 30 m deeper than in the data at the second observed SST wake, a time when WPi was ~4 (Figure 2f). In these conditions, Figure 8a shows that the SST response is around -2°C for a H2 ~ 50 m and -0.5°C for a H2 ~ 80 m. Hence, the H2 model bias at that time and location before the Ketsana passage gives a plausible explanation for the model data discrepancy in Figure 2.

Another feature of Figure 2 is the similar response in cooling amplitude for both cyclones but a contrast in chlorophyll response, with no bloom for Parma and a weak bloom for Ketsana. Figure 8a indicates shallow H2 (42 m for Parma and 66 m for Ketsana) and strong WPi values (4.3 for Parma and 5.7 for Ketsana) for both cyclones, promoting a relatively strong cold wake for both cyclones (~-2° to -2.5°C according to Figure 8a).

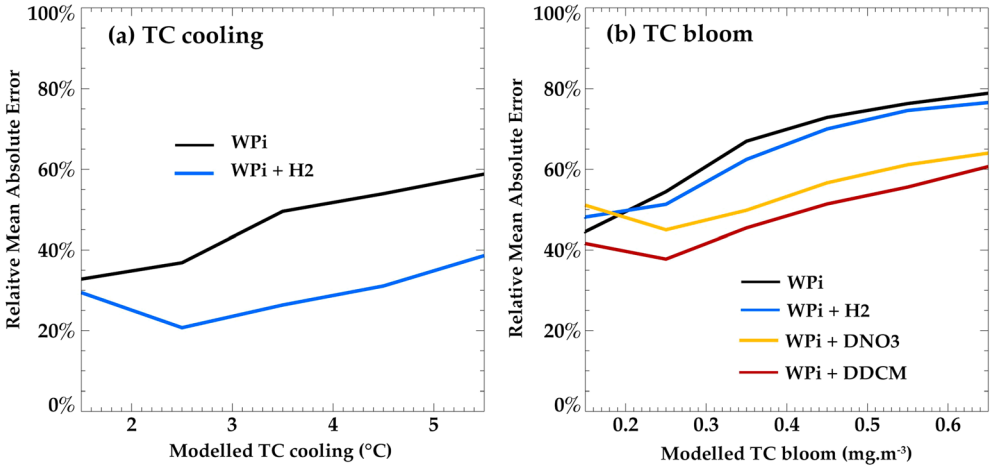

Figure 9. Relative mean absolute error (mean absolute error divided by the value of the predicted variable, expressed as a percentage) of a prediction of (a) the simulated cooling using WPi as a single predictor (black) and WPi and H2 as a couple of predictors (blue) and (b) the simulated bloom using WPi as a single predictor (black), WPi and H2 (blue), WPi and DNO_3 (orange), and WPi and DDCM (red) as a couple of predictors.

Ketsana cooling is larger than the one calculated from the binned response (−3°C against −2°C in Figure 8a, illustrating the dispersion of the modeled responses for a given bin, see above), while Parma cooling is slightly lower (−2°C against −2.5°C), but both are within the range of the moderate cooling predicted from relatively strong WPi and shallow H2. The weak chlorophyll responses under both TCs (Figure 2) largely arise from the fact that they occur over very deep DCM and nitracline (~150 m; Figure 8b). Figures 8b and 8c also show that in the WPi range occupied by Parma, its chlorophyll response is expected to be very weak as was observed, while Ketsana chlorophyll response is expected and observed to be a bit stronger because of a larger WPi.

We more precisely assess the combined control of the amplitude of the modeled surface ocean response by the TC energy input and oceanic background state as follows. We first fit Figure 8's responses (R) as a function of the WPi and the oceanic parameter P (P is H2 when fitting cold wakes and P is DNO_3 or DDCM when fitting chlorophyll wakes). We use a linear fit of the response R (cold wake of chlorophyll) to the WPi alone ($R_\text{fitted} = c_0 + c_1$ WPi) as a reference. We use a bivariate first-order polynomial fit ($R_\text{fitted} = c_0 + c_1$ WPi $+ c_2$ P $+ c_3$ WPi $\times P$) to quantitatively estimate the control of the response R by oceanic parameters. We then apply these fits to the individual TC parameters and compare the TC fit to the actual TC response by estimating an error $|R_\text{fitted}\ (\text{TC}) - R\ (\text{TC})|$. We then average these errors as functions of the cooling (1°C wide bins) and chlorophyll (0.1 mg m^{-3} bins) responses to show the error dependence to the TC response amplitude. The results are referred to as "mean absolute errors" (MAE) and shown in Figure 9 as percentages of the cooling/chlorophyll responses.

Figure 9 assesses the improvement brought by the inclusion of the oceanic parameters by comparing the MAEs (expressed in % in the following by dividing by the value of the predictor) of the bivariate versus univariate statistical models versus the original TC-induced responses. As shown in Figure 9a and already discussed by *Vincent et al.* [2012a], including H2 clearly reduces the error of the predicted cooling compared to using WPi alone. For instance, using WPi alone yields a relative error on the cooling prediction of 40% for a −2.5°C cooling reducing to 20% when using WPi and H2 (Figure 9a). Similarly, using DDCM along with WPi results in an error reduction compared to using WPi alone (Figure 9b) for the entire range of bloom amplitudes. Using DNO_3 also results in a significant error reduction although slightly weaker than that of DDCM. In contrast, using H2 in addition to WPi only marginally improves the predicted bloom amplitude. The above analysis therefore demonstrates quantitatively that ocean biogeochemical parameters such as the nitracline depth or the depth of the DCM control a significant part of the bloom amplitude, in combination with the level of energy input to the ocean by the TC, as measured by WPi. It must however be acknowledged that the quality of the best cooling prediction (blue curve in Figure 9a) is better than the quality of the best bloom prediction (red curve in Figure 9b).

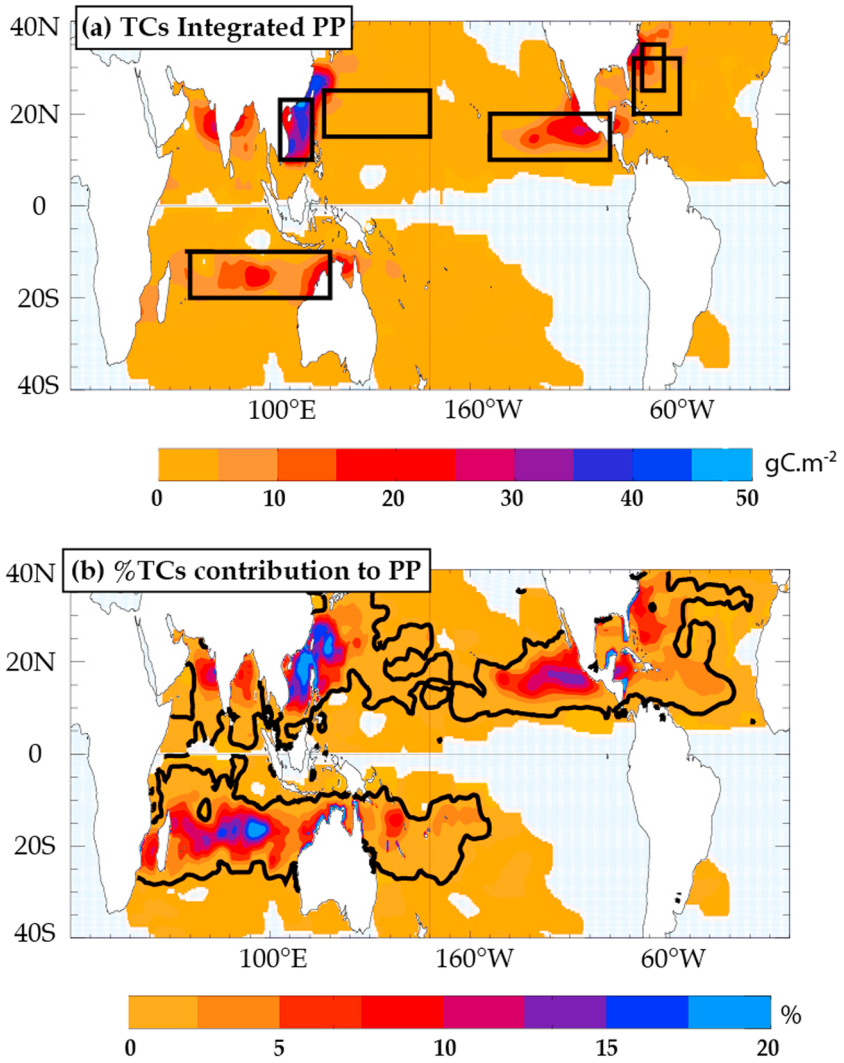

Figure 10. Spatial map of (a) time-integrated TC-induced primary production (in gC m^{-2}) from 3 days before to 60 days after the cyclone passage and (b) same as above but in percentages of the annual mean primary production. In Figure 10a, the four overlaid boxes (two boxes in the Northwestern Pacific and two in the North Atlantic; one in the Southern Indian Ocean and one in the Eastern Pacific) correspond to areas referenced in Table 1 and in Figure 11. In Figure 10b, the contour of 0.5% is also added in black.

5. Climatological Impact

Finally, our modeling framework also allows us to characterize the overall TC impacts on vertically integrated (see section 2) primary production (PP) by spatially integrating all modeled PP responses in 200 km radius disks around TC positions, as was done for SST and chlorophyll in Figure 5. In addition, we also calculate the time integral of that PP from 3 days before to 60 days after the cyclone passage. The time integration allows characterizing the net impact of the TCs on PP. While a maximum of 30 days was used in the previous sections, in this case we wish to integrate under the TCs long enough to be sure to include the overall time effect of the TCs. Changing 60 days to another reasonable value (50, 70, etc.) does not change the results as most effects are in fact contained in the first 30 days after TC passages. Mean spatial maps for this time-integrated PP are shown in Figure 10.

As expected, Figure 10a mimics Figure 5d since chlorophyll and primary production spatial patterns are strongly tied. First, one sees that the areas of significant TC impacts are very limited, while the vast majority of TC-affected regions show below 5 gC m^{-2} TC-induced primary production. The areas of significant TC impacts are essentially found in the North Eastern Pacific, the South China Sea, north and northwest of the

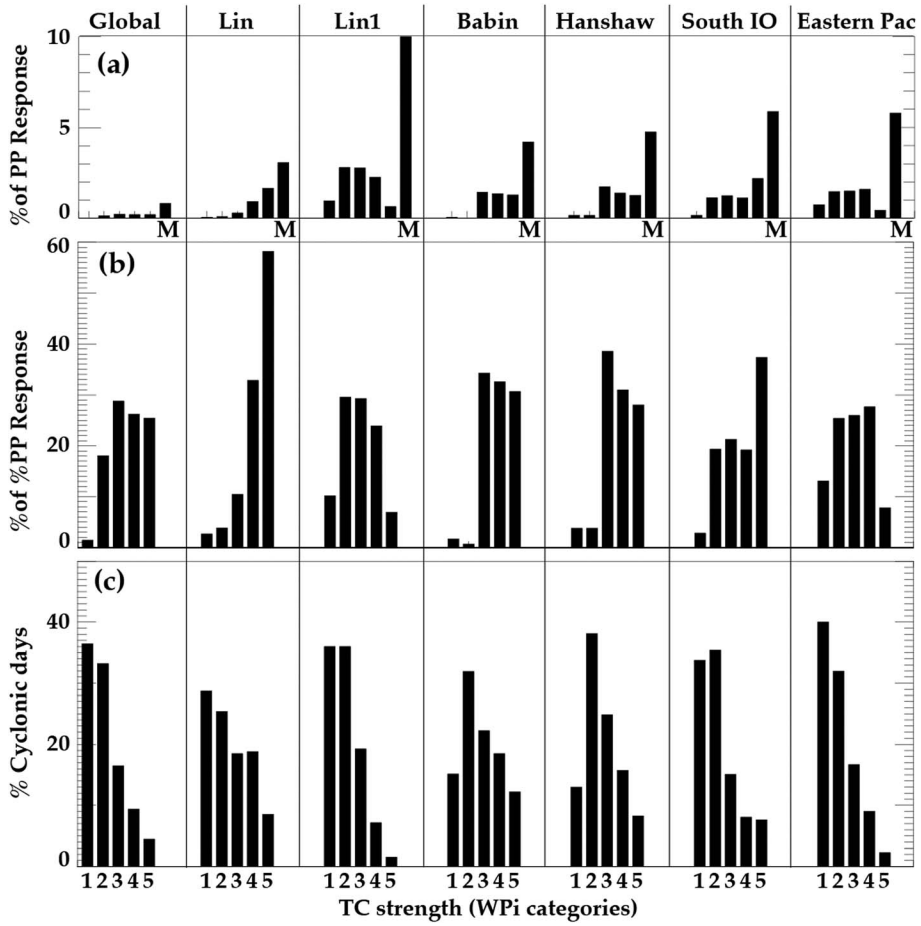

Figure 11. (a) Percentage of TC induced primary production to the annual mean production in the boxes defined in Table 1 and framed in Figure 10a. In each box, the percentage is broken down into the contribution by WPi category (1 to 5 labeled in abscissa) as well as the average over all categories (labeled M on the abscissa in Figure 11a) when needed. (b) The same boxplot as Figure 11a is produced but each category is scaled by the mean over all categories ("M" in Figure 11a) and is expressed in %. (c) The % of cyclone days entering each WPi categories.

Australian coast, the South Tropical Indian Ocean, the eastern side of the Arabian Sea, the western side of the Bay of Bengal, and the Northwest Atlantic. In the South China Sea, for instance, TC induce a ~40 $gC\,m^{-2}$ production each year (Figure 10a). When expressed in terms of percentage of the annual mean production (Figure 10b), this TC-related PP shows vast areas with less than 0.5% impacts. In other regions, the TC impacts can reach ~20–30% locally in the South China Sea, up to 20% near the Australian coast and in the South Indian ridge region, and at most 15% in the North Eastern Pacific region.

Figure 11 further illustrates the contribution of each TC category to their climatological signature in a series of selected regions (Figure 10a and see Table 1 for their spatial extent). The global average of Figure 10b shows that the TC-induced impact on the global scale is ~1% of the annual production (Figure 11a) because of the vast regions with very low impacts. While Cat 1 and Cat 2 TCs account for ~70% of the global TCs days (Figure 11b), they only contribute to 20% of the TC climatological impacts. Cat 3, 4, and 5 TCs, which only account for 30% of global TC days (Figure 11c), contribute to 80% of the total response. Figure 11 also shows that these numbers vary regionally. In the North Pacific ("Lin" box) and Atlantic regions ("Babin" and "Hanshaw" boxes), weak TCs (Cat 1 and 2) only very marginally contribute (<6%, Figure 11b) to the weak total response (Figure 11a), while their contribution is larger for the South China Sea ("Lin1" box), South Indian Ocean and Eastern Pacific regions (25 to 40%). The spatial distribution of the climatological depth of the nitracline and the chlorophyll maximum can largely explain this different contribution of weak TCs. In oligotrophic regions such as the North Pacific and Atlantic regions, the depth of the nitracline and of the deep chlorophyll

Table 1. Names, Latitudes, and Longitudes of the Boxes Used in Figures 10 and 11[a]

Domain of Average	Averaged WPi Value
Global (40°S–40°N) under all TC-prone areas	2
[127°E–180°/15°N–25°N] [*Lin*, 2012] referenced as Lin in the text	2.4
[105°E–121°E/10°N–23°N] [*Lin et al.*, 2003] referenced as Lin1 in the text	1.9
[78°W–55°W/20°N–32°N] [*Babin et al.*, 2004] referenced as Babin in the text	2.6
[74°W–63°W/25°N–35°N] [*Hanshaw et al.*, 2008] referenced as Hanshaw in the text	2.5
[60°E–130°E/20°S–10°S] South Indian Ocean	2.1
[150°W–90°W/10°N–20°N] Eastern Pacific	1.9

[a]Some are labeled from the studies of *Lin* [2012] (box Lin), *Lin et al*. [2003] (box Lin1), *Babin et al*. [2004] (box Babin), and *Hanshaw et al*. [2008] (box Hanshaw). Second row, averaged WPi values in these boxes.

maximum are very deep (>150 m; Figures 6c–6f) and mixing induced by weak TCs is not energetic enough to reach such a depth, resulting in a very weak contributions. In the South China Sea, the South Indian Ocean, and the Eastern Pacific, they are considerably shallower (50–80 m) resulting in a significant chlorophyll response even for weak TCs.

6. Discussion and Conclusion

Several studies already documented TCs chlorophyll response from satellite observations, but there is no consensus on the mechanisms driving these blooms and on the TCs global contribution to annual primary production. This largely arises from the diversity in the considered methodologies, data sets, time periods, and regions studied. In the present paper, we revisit these questions using a global approach over a long time period (~10 years), by combining satellite observations and numerical model results. We extract the chlorophyll response to more than 1000 TCs over the 1998–2007 period from both satellite data and a coupled dynamical-biogeochemical simulation in which a realistic cyclonic forcing is inserted. This approach allows characterizing the robust features of the blooms under TCs as well as to map out their climatological chlorophyll and primary production response globally. The model is then used to discuss the mechanisms driving these results.

In addition to the classic cold wake under TCs, cyclones on average induce a modest chlorophyll bloom of ~0.025 mg m^{-3} in the satellite data and 0.05 mg m^{-3} in the model in their wake, 2–6 days after the cyclone passage lagging the cold wake by 1 day. This weak averaged response however masks a large diversity. Most TCs indeed induce very weak blooms (60% of the responses range between −0.02 and 0.02 mg m^{-3}), while ~10% of the TCs induce blooms larger than 0.1 mg m^{-3}.

The observations and model analyses both indicate that most of the strongest blooms occur near the coasts in TC-prone regions. In contrast, TC-induced coolings occupy much wider regions and extend more into the open ocean. The TC contribution to vertically integrated primary production has very similar spatial patterns to those of TC-induced chlorophyll blooms. On average over all TC-prone regions, TCs induce a very modest (~1%) contribution to the annual primary production. This small contribution is however regionally contrasted and can reach up to 20–30% in the South China Sea locally, 20% in the South Tropical Indian Ocean and along the coast of Northern Australia, and 15% in the Eastern Pacific, locally. TC categories do not all have the same impacts and their impact vary regionally because the wake amplitudes are controlled by both the TC energy input—whose partition into cyclone categories is regionally dependent—and the ocean preconditioning.

Indeed, as already acknowledged in several other studies [*Lloyd and Vecchi*, 2010; *Vincent et al.*, 2012a], the amplitude of TC energy input to the ocean and the strength upper ocean stratification are the most important factors controlling the amplitude of the cold wakes. Here we show that the amplitude of TC-induced blooms is also largely driven by TC wind energy input and the depth of the nitracline/deep chlorophyll maximum. Stronger blooms are mostly found in regions of intense TCs and where the nitracline depth and/or the deep chlorophyll maxima are shallow (<60 m). Most open ocean regions exhibit deep nitracline and subsurface chlorophyll maxima (100 m or more) explaining why the chlorophyll responses are rather weak there. In contrast, coastal upwelling regions generally have a shallower nitracline and subsurface chlorophyll maximum allowing for large blooms in coastal areas. The shallow upper ocean thermal stratification compared

to a relatively deep nitracline/subsurface chlorophyll maximum in open ocean regions explains why large TC-induced coolings but weak chlorophyll responses occur in these regions.

Assessments of the TCs climatological impact on chlorophyll or primary production have already been attempted by a few studies using satellite observations [*Lin et al.*, 2003; *Babin et al.*, 2004; *Hanshaw et al.*, 2008; *Lin*, 2012] and the conclusions are contrasted. *Lin* [2012] estimated a negligible 0.15% TC contribution to the global annual mean anthropogenic CO_2 uptake in the western North Pacific from the analysis of 11 typhoons in 2003. We also find a weak TC contribution of 3% to the annual production in the same region (Lin box, Figure 11). Extrapolating from one TC during 2000, *Lin et al.* [2003] suggested that TC contributions could amount to 20–30% of the annual mean production in the South China Sea. Instead, we find a mean contribution of ~10% in the region but the model also shows localized areas of higher TC contributions. The only previous study really exploring the climatological impact of TCs on primary production over a sufficiently long period is the one from *Hanshaw et al.* [2008] for the North Atlantic, investigating the 1997–2005 period from SeaWiFS data. They concluded that TCs have a minimal effect ($<$1%) on the annual chlorophyll biomass there because of their limited spatial extension and occurrence. In our model context and over the 1998–2007 period, we find a 5% contribution of TCs to primary production (Figure 11a) and a 2% contribution of TCs to surface chlorophyll in the box that *Hanshaw et al.* [2008] studied. Our model hence generally agrees with observations in suggesting a weak TC contribution to the annual mean production. We also agree with that study in designating the episodic character of the cyclones as one reason for such a small contribution. A second reason is however that the open ocean deep nitracline and maximum chlorophyll depths prevents a more widespread strong chlorophyll and primary production response. *Babin et al.* [2004] examined 13 hurricanes in a region close as that used in *Hanshaw et al.* [2008] and from 1998 to 2001. They found, with a relatively large spread in the chlorophyll responses ranging from 5% to 91% increase relative to the background value, a diversity that our model allows to understand given that *Babin et al.*'s [2004] box contains both shallow DDCM/DNO_3 (favorable to significant responses) at its western edge and deep $DDNO_3$/DDCM (unfavorable to responses) in its eastern side. Yet when moving to a climatological assessment, in our model context, we also conclude that the maximum TC contribution to production in *Babin et al.*'s [2004] box is weak (~5%, Figure 11a).

We have shown that the TC contribution to primary production, although weak, has strong regional variations (Figure 10) depending on both the TC characteristics and the oceanic biogeochemical background. That stresses the difficulty of extrapolating the global or regional PP impact of TCs from a single cyclone [e.g., *Lin et al.*, 2003]. In addition, even with similar TC characteristics and oceanic conditions, the dispersion of the TC response remains high in the model so that it does not seem possible to predict the exact chlorophyll response to an individual TC (Figures 8 and 9) but rather a range of responses. Our results finally stress that regional budgets will crucially depend on the exact delimitation of the regions because the chlorophyll/primary production TC patterns are very regionally confined, especially near the coasts.

An obvious caveat of our study lies in the larger modeled chlorophyll response compared to observations (Figure 3). This mismatch does not arise from the numerous missing values existing in the satellite data under the TC eye due to high cloud cover, since subsampling the data with only observed pixels does not affect the comparison. This mismatch may come from the limitations of the ocean color algorithm retrieval (here the GSM model from Globcolour). Near the coastal influence, for instance, the chlorophyll retrieval can be biased by particle of all sorts, sediment resuspension under TC dynamics, and colored dissolved organic matter. Since we use a relatively low resolution observational data set (25 km), chlorophyll retrievals should not be strongly affected more than 1–2 pixels away from the coasts but our results should anyway be regarded with caution in coastal regions. Second, under heavily clouded skies such as those occurring under TCs, it may also well be that the model forcing does not reproduce the short wave reduction under the TCs, which would intuitively result in a bloom overestimation by the model under TCs. To ascertain this, we performed a composite evolution of cloud fraction under TCs from the Globcolour cloud fraction data sets (not shown): this analysis reveals that the cloud cover increases from ~65% 10 days before the TC passage to ~90% at the time the TC passes and drops back to the background conditions ~3 days after. Based on the literature [for instance, *Frouin and Pinker*, 1995], such a 25% increase would not significantly affect primary production. In the model, a similar composite of the short wave radiation forcing also displays a short wave reduction from the 230 W m^{-2} down to 170 W m^{-2} at the cyclone passage, consistent with the observed cloud cover increase [*Reed*, 1977]. The discrepancies between the model and observations hence lie somewhere else.

This bias can indeed also arise from model caveats, including the sensitivity to model biogeochemical parameterization and/or to the atmospheric forcing used. If this bias is arising from model caveats, the conclusion remains that the actual TC contribution to primary production must be small in most regions (Figures 10 and 11), since the model is biased toward stronger responses.

The lack of clear understanding of mechanisms driving the blooms under TCs has been pointed out by *Babin et al.* [2004]. Unraveling detailed mechanisms for these blooms in the model requires the examination of the chlorophyll equation as other authors did for the SST equation [e.g., *Jullien et al.*, 2012; *Vincent et al.*, 2012a]. Unfortunately, we do not have access to that in our simulations. However, the equal importance of the nitracline and subsurface chlorophyll maximum depth in setting the chlorophyll response points toward processes such as vertical mixing/advection of nutrients or direct injection of the deep chlorophyll maximum into the euphotic layer as major drivers of chlorophyll blooms under TCs as previously suggested by *Babin et al.* [2004] in their data analyses. The strong correlation between the depth of the nitracline and the subsurface chlorophyll maximum under TCs (~0.9) does however not allow us to discriminate between these two processes. TC-induced new production patterns (not shown) are nevertheless similar to primary production patterns (Figure 10). That shows that the injection of new nitrate into the photic layer is an active mechanism setting the TC chlorophyll response. The chlorophyll under TCs also displayed a significant percentage of weak negative responses in data and observations with reduced chlorophyll rather than enhanced chlorophyll (Figure 4). Unlike the positive responses, the vast majority of these weak negative responses appear off the coasts in regions of deeper nitracline and chlorophyll maxima ($\sim > 80$ m, not shown). In these regions, it is possible that TC mixing, while not strong enough to reach the DDCM or DNO_3, dilutes surface chlorophyll by bringing deeper oligotrophic water and/or forcing downward surface waters. Other mechanisms could also be invoked. *Vincent et al.* [2012a] explored the details of the heat equation and concluded that although of secondary importance, the role of horizontal advection contributes to ~10% of the cooling amplitude for the largest wind forcing. Based on these conclusions, it is hence plausible that horizontal advection locally plays a role, especially in coastal areas, where strong horizontal gradients of chlorophyll (Figure 1) and nutrients (Figure 6) are found.

We have used a global 0.5° resolution dynamical-biogeochemical model in conjunction to daily 25 km GLOBCOLOUR data to explore the individual response of chlorophyll/primary production to tropical cyclones as well as the their climatological impacts. The SST and chlorophyll responses to TCs display spatial scales of ~250 km at least in both our study and the literature. The choice of a 25 km resolution for the ocean color data, instead of higher available resolutions such as 9 or 4 km, thus seems reasonable. Our model assessment may depend on the model horizontal resolution. For instance, *Vincent et al.* [2012b] examined the Ekman pumping induced by TCs for a variety of model resolution ranging from 2° to 1/12° (see their Figure 2 and concluding remarks). They showed that the ½° model missed ~30% of the Ekman pumping compared to the 1/4°. They however concluded that based on the fair agreement between the observed and modeled SST responses, a ½° resolution was an acceptable compromise between the model quality and computational cost. Other processes are impacted by horizontal resolution such as advection and vertical mixing. In our case, adding the biological model prevented to increase the resolution of the global model beyond ½° but additional studies dedicated to resolution issues on case studies could be undertaken to understand the impact of resolution onto biological responses under TCs.

Finally, our study quantified the climatological impact of TCs on chlorophyll and primary production globally but could not conclude on the detailed mechanisms by which TCs can enhance or decrease surface chlorophyll. Such quantitative assessment would require to output the 3-D ecosystem equation terms at high frequency and to perform analyses such those that [*Jullien et al.*, 2012; *Vincent et al.*, 2013] did on the temperature equation.

Acknowledgments
The authors thank IRD and CNRS for salary support, as well as the data providers for free data access. The authors also thank P. Leognan and N. Saint-Georges in the realization of the model experiments. C. Menkes also thank Robert Frouin and anonymous reviewers for their patience as well as for very detailed and helpful reviews. The data used here are accessible upon request to C. Menkes.

References

Aumont, O., and L. Bopp (2006), Globalizing results from ocean in situ iron fertilization studies, *Global Biogeochem. Cycles*, *20*, GB2017, doi:10.1029/2005GB002591.

Babin, S. M., J. A. Carton, T. D. Dickey, and J. D. Wiggert (2004), Satellite evidence of hurricane-induced phytoplankton blooms in an oceanic desert, *J. Geophys. Res.*, *109*, C03043, doi:10.1029/2003JC001938.

Donelan, M. A., B. K. Haus, N. Reul, W. J. Plant, M. Stiassnie, H. C. Graber, O. B. Brown, and E. S. Saltzman (2004), On the limiting aerodynamic roughness of the ocean in very strong winds, *Geophys. Res. Lett.*, *31*, L18306, doi:10.1029/2004GL019460.

Emanuel, K. (2001), Contribution of tropical cyclones to meridional heat transport by the oceans, *J. Geophys. Res.*, *106*, 14,771–14,781, doi:10.1029/2000JD900641.

Emanuel, K. (2005), Increasing destructiveness of tropical cyclones over the past 30 years, *Nature*, *436*(7051), 686–688, doi:10.1038/nature03906.

Foltz, G. R., K. Balaguru, and L. R. Leung (2015), A reassessment of the integrated impact of tropical cyclones on surface chlorophyll in the western subtropical North Atlantic: A reassessment of the integrated impact of tropical cyclones on surface chlorophyll in the western subtropical North Atlantic, *Geophys. Res. Lett.*, *42*, 1158–1164, doi:10.1002/2015GL063222.

Frouin, R., and R. T. Pinker (1995), Estimating photosynthetically active radiation (PAR) at the Earth's surface from satellite observations, *Remote Sens. Environ.*, *51*(1), 98–107, doi:10.1016/0034-4257(94)00068-X.

Griffies, S. M., et al. (2009), Coordinated Ocean-ice Reference Experiments (COREs), *Ocean Model.*, *26*(1–2), 1–46, doi:10.1016/j.ocemod.2008.08.007.

Hanshaw, M. N., M. S. Lozier, and J. B. Palter (2008), Integrated impact of tropical cyclones on sea surface chlorophyll in the North Atlantic, *Geophys. Res. Lett.*, *35*, L01601, doi:10.1029/2007GL031862.

Jullien, S., C. E. Menkes, P. Marchesiello, N. C. Jourdain, M. Lengaigne, A. Koch-Larrouy, J. Lefèvre, E. M. Vincent, and V. Faure (2012), Impact of tropical cyclones on the heat budget of the South Pacific Ocean, *J. Phys. Oceanogr.*, *42*(11), 1882–1906, doi:10.1175/JPO-D-11-0133.1.

Jullien, S., P. Marchesiello, C. Menkes, J. Lefevre, N. Jourdain, M. Lengaigne, and G. Samson (2014), Ocean feedback on tropical cyclone intensity in a multidecadal coupled simulation of the South Pacific, vol. 16, p. 14939.

Large, W. G., and S. G. Yeager (2009), The global climatology of an interannually varying air–sea flux data set, *Clim. Dyn.*, *33*(2–3), 341–364, doi:10.1007/s00382-008-0441-3.

Lévy, M., M. Lengaigne, L. Bopp, E. M. Vincent, G. Madec, C. Ethé, D. Kumar, and V. V. S. S. Sarma (2012), Contribution of tropical cyclones to the air-sea CO_2 flux: A global view, *Global Biogeochem. Cycles*, *26*, GB2001, doi:10.1029/2011GB004145.

Lin, I., W. T. Liu, C.-C. Wu, G. T. F. Wong, C. Hu, Z. Chen, W.-D. Liang, Y. Yang, and K.-K. Liu (2003), New evidence for enhanced ocean primary production triggered by tropical cyclone, *Geophys. Res. Lett.*, *30*(13), 1718, doi:10.1029/2003GL017141.

Lin, I.-I. (2012), Typhoon-induced phytoplankton blooms and primary productivity increase in the western North Pacific subtropical ocean, *J. Geophys. Res.*, *117*, C03039, doi:10.1029/2011JC007626.

Lloyd, I. D., and G. A. Vecchi (2010), Observational evidence for oceanic controls on hurricane intensity, *J. Clim.*, *24*(4), 1138–1153, doi:10.1175/2010JCLI3763.1.

Madec, G. (2008), NEMO ocean engine. [Available at http://nora.nerc.ac.uk/164324/], (Accessed 4 August 2014).

Mei, W., C. Pasquero, and F. Primeau (2012), The effect of translation speed upon the intensity of tropical cyclones over the tropical ocean: TC translation speed affects intensity, *Geophys. Res. Lett.*, *39*, L07801, doi:10.1029/2011GL050765.

Menkes, C. E., M. Lengaigne, P. Marchesiello, N. C. Jourdain, E. M. Vincent, J. Lefèvre, F. Chauvin, and J.-F. Royer (2012), Comparison of tropical cyclogenesis indices on seasonal to interannual timescales, *Clim. Dyn.*, *38*(1–2), 301–321, doi:10.1007/s00382-011-1126-x.

Moore, C. M., et al. (2013), Processes and patterns of oceanic nutrient limitation, *Nat. Geosci.*, *6*(9), 701–710, doi:10.1038/ngeo1765.

Neetu, S., M. Lengaigne, E. M. Vincent, J. Vialard, G. Madec, G. Samson, M. R. Ramesh Kumar, and F. Durand (2012), Influence of upper-ocean stratification on tropical cyclone-induced surface cooling in the Bay of Bengal, *J. Geophys. Res.*, *117*, C12020, doi:10.1029/2012JC008433.

Reed, R. K. (1977), On estimating insolation over the ocean, *J. Phys. Oceanogr.*, *7*(3), 482–485, doi:10.1175/1520-0485(1977)007<0482:OEIOTO>2.0.CO;2.

Shiah, F.-K., S.-W. Chung, S.-J. Kao, G.-C. Gong, and K.-K. Liu (2000), Biological and hydrographical responses to tropical cyclones (typhoons) in the continental shelf of the Taiwan Strait, *Cont. Shelf Res.*, *20*(15), 2029–2044, doi:10.1016/S0278-4343(00)00055-8.

Vincent, E. M., M. Lengaigne, J. Vialard, G. Madec, N. C. Jourdain, and S. Masson (2012a), Assessing the oceanic control on the amplitude of sea surface cooling induced by tropical cyclones, *J. Geophys. Res.*, *117*, C05023, doi:10.1029/2011JC007705.

Vincent, E. M., M. Lengaigne, G. Madec, J. Vialard, G. Samson, N. C. Jourdain, C. E. Menkes, and S. Jullien (2012b), Processes setting the characteristics of sea surface cooling induced by tropical cyclones, *J. Geophys. Res.*, *117*, C02020, doi:10.1029/2011JC007396.

Vincent, E. M., G. Madec, M. Lengaigne, J. Vialard, and A. Koch-Larrouy (2013), Influence of tropical cyclones on sea surface temperature seasonal cycle and ocean heat transport, *Clim. Dyn.*, *41*(7-8), 2019–2038, doi:10.1007/s00382-012-1556-0.

Wentz, F. J., C. Gentemann, D. Smith, and D. Chelton (2000), Satellite measurements of sea surface temperature through clouds, *Science*, *288*(5467), 847–850, doi:10.1126/science.288.5467.847.

Willoughby, H. E., and M. E. Rahn (2004), Parametric representation of the primary hurricane vortex. Part I: Observations and evaluation of the Holland (1980) model, *Mon. Weather Rev.*, *132*(12), 3033–3048, doi:10.1175/MWR2831.1.

Willoughby, H. E., R. W. R. Darling, and M. E. Rahn (2006), Parametric representation of the primary hurricane vortex. Part II: A new family of sectionally continuous profiles, *Mon. Weather Rev.*, *134*(4), 1102–1120, doi:10.1175/MWR3106.1.

Zhang, S., L. Xie, Y. Hou, H. Zhao, Y. Qi, and X. Yi (2014), Tropical storm-induced turbulent mixing and chlorophyll-*a* enhancement in the continental shelf southeast of Hainan Island, *J. Mar. Syst.*, *129*, 405–414, doi:10.1016/j.jmarsys.2013.09.002.